



CHORUS

This is the accepted manuscript made available via CHORUS. The article has been published as:

Evolution of pair correlation symmetries and supercurrent reversal in tilted Weyl semimetals

Mohammad Alidoust and Klaus Halterman

Phys. Rev. B **101**, 035120 — Published 13 January 2020

DOI: [10.1103/PhysRevB.101.035120](https://doi.org/10.1103/PhysRevB.101.035120)

Evolution of Pair Correlation Symmetries and Supercurrent Reversal in Tilted Weyl Semimetals

Mohammad Alidoust¹ and Klaus Halterman²

¹*Department of Physics, Norwegian University of Science and Technology (NTNU), NO-7491, Trondheim, Norway*

²*Michelson Lab, Physics Division, Naval Air Warfare Center, China Lake, California 93555, USA*

(Dated: November 4, 2019)

We study the effective symmetry profiles of superconducting pair correlations and the flow of charge supercurrent in ballistic Weyl semimetal systems with a tilted dispersion relation. Utilizing a microscopic method in the ballistic regime and starting from both *opposite*-pseudospin (the band degree of freedom) and *equal*-pseudospin phonon-mediated opposite-spin electron-electron couplings, we calculate the anomalous Green's function to study various superconducting pair correlations that Weyl semimetal systems may develop. The momentum-space profile reveals that by properly manipulating the parameters of Weyl semimetal systems, including the tilting parameter, the effective symmetry class of even-parity *s*-wave (odd-parity *p*-wave) superconducting correlations can be converted into a *d*-wave (*f*-wave) symmetry class that consists of equal-pseudospin and opposite-pseudospin channels. We also find that the supercurrent in a ballistic Weyl Josephson junction can be made to vanish or switch directions, depending on the tilt of the Weyl cones, in addition to the relevant parameters characterizing the Weyl semimetal and junction. We show that inversion symmetry breaking terms introduce transitions that result in the appearance of self-biased current at zero difference between the macroscopic phases of the superconducting segments, creating a φ_0 Josephson state. Weyl semimetal systems are shown to offer several experimentally tunable parameters to control the induction of higher harmonics into the current phase relations.

I. INTRODUCTION

A Weyl semimetal (WS) is a topologically nontrivial phase of matter that has been heavily pursued experimentally and theoretically.¹⁻³ The band structure in these materials exhibits Weyl points, where the conduction and valence bands intersect. Around these points, the energy dispersion of the quasiparticle excitations has a conical profile. The Weyl points only appear in pairs, which are identified by Weyl fermions in real space, or a source or sink of Berry curvature in momentum space.^{4,5} This topological phase results in the band structure in the bulk of Weyl semimetals being gapless, although Fermi arc states connect pairs of Weyl points.⁶ As has been widely discussed, the presence of gapless surface states opens up transport channels free from backscattering. For a conventional type-I WS, the Fermi surface is point-like, where electron and hole states occupy separate energy ranges above or below the Weyl point.⁷ By tilting the Weyl cones through the tilt parameter β , a type-II WS emerges with an open Fermi surface containing electron and hole pockets near the Weyl points.⁸ Recently, some experimental signatures of the type-II WS phase have been reported.⁹ Also, the optical properties of type-II WSs have been investigated,¹⁰⁻¹³ including how tilt affects optical conductivity¹⁰, absorption^{11,13}, and Hall conductivity.¹²

If the Weyl semimetal is intrinsically superconducting, or becomes so through proximity effects, it can host surface-localized Majorana fermions with zero energy.^{14,26,28} Since Majorana fermions follow non-Abelian statistics and are their own antiparticles, superconducting Weyl systems are anticipated to play a promising role in topological quantum computing.¹⁵⁻¹⁸ Experimentally, superconductivity in Weyl materials has been discovered in a variety of settings, including in MoTe₂ under pressure, and in TaAs by photoemission spectroscopy.^{19,20} It was reported that surface superconductivity can be induced in NbAs through ion irradiation.²¹ Re-

cently, Nb-doped Bi₂Se₃ and the heavy fermion superconductor UPt₃ were predicted to be Weyl superconductors.²² Apart from naturally occurring materials, superconductivity in Weyl semimetals may also be realized through doping²³⁻²⁵. These intriguing phenomena have motivated a significant wave of interest to the Weyl metal systems both theoretically and experimentally.^{19,26-30,33-65}

When discussing the superconducting state of a Weyl semimetal, the symmetry of the electron-electron coupling potential, Δ , is an important property that gives insight into the nature of the pairing correlations. Moreover, when a relationship exists between the quasiparticle excitations in the Weyl phase and the pair correlations, a more complete understanding of the underlying electronic structure can be obtained. As a typical example, hybrid superconducting systems containing inhomogeneous ferromagnets can generate odd-frequency equal-spin triplet pairs. In these systems, the triplet pairs are accompanied by a zero energy peak in the density of states, which might be a signature of spin-triplet superconducting correlations. For an overview of this phenomenon see Refs. 66-71 and references therein. The dominant pairing symmetry in a system however, depends on many factors, including the band structure and strength of the pairing interactions. Thus, by implementing complimentary experimental probes that identify thermodynamic or spectroscopic signatures, the pairing symmetries and associated pairing mechanisms and types of interactions can be clarified.

A macroscopic quantum effect that can reveal experimental signatures of the electronic properties of the Weyl semimetal is the Josephson current, which arises from a phase difference across two superconducting segments in a junction. Applications involving Josephson junctions has grown due to their impact and potential improvements in next generation superconducting computing, nonvolatile memories, and magnetometers,⁷² where single flux quantum circuits contain numerous arrangements of Josephson junctions to improve

speed and sensitivity. To determine the thermodynamic properties of practical cryogenic Weyl devices, it is crucial to understand the behavior of charge current flow in these types of systems.

This paper contains two main parts. Since the superconducting pair correlations can reveal hints of the host material, including lattice interactions, electronic structure, and pairing mechanism, the symmetry of the superconducting correlations can play a significant role in most experimental tests. Thus, first we study the symmetry profiles of the superconducting correlations that a tilted WS (in the type-I and type-II phases) might develop through opposite-pseudospin (Pspin - the band degree of freedom) and equal-pseudospin phonon-mediated opposite-spin electron-electron coupling. In order to study the symmetries of the superconducting correlations, we construct the Green's function in the ballistic regime. We derive analytical expressions for the Green's function components and explore both analytically and numerically the behavior of the pair correlations for a variety of WS system parameters. Our results show that, depending on the parameters, a WS can support superconducting pair correlations with effective s -wave and p -wave symmetry classes that are even-parity and odd-parity, consisting of opposite-Pspin and equal-Pspin channels. Importantly, we find that by properly tuning the parameters of a WS, including the tilting parameter β , the effective s -wave and p -wave symmetry classes can evolve into d -wave and f -wave classes. Thus, our results suggest that this type of superconducting WS platform can serve as a "switch" that converts the symmetry classes of the superconducting correlations. These predictions can be confirmed by high resolution angular point-contact spectroscopy experiments or Meissner-effect based experiments that are suitable to perform the directional-dependency of superconducting correlations. The findings here may also stimulate further studies involving scenarios similar to a recent experiment where superconductivity in a Weyl semimetal subject to external strain was studied⁶⁵.

The second part of this paper is devoted to the transport of dissipationless charge current. We make use of wavefunctions derived from an exact diagonalization of the Bogoliubov-de Gennes Hamiltonian, without applying any simplifying approximations. A phase difference φ is established across a Josephson junction to study the behavior of the supercurrent in a superconductor (S)-normal metal (N)-superconductor (S) junction. We consider the situation where superconductivity arises from unequal spin quasiparticles belonging to different Pspins. We find that by varying various parameters, including β , and the inversion breaking parameters of the WS, the system can experience a transition whereby the current reverses direction and changes its periodicity from 2π to 4π at the reversal points. The inclusion of a proper inversion breaking parameter creates a situation where a self-biased current can flow through the junction with $\varphi = 0$, creating a φ_0 Josephson state. Our results demonstrate that the self-biased supercurrent is controllable by different parameters of the WS junction, including β and junction length. In contrast to previous works where an exchange field is a necessary ingredient^{28,29,77-79}, the φ_0 state explored here relies on inherent parameters of

the WS Josephson junction independent of the density of non-magnetic impurities and disorder that might be introduced in the system²⁷. Our results in the ballistic regime are consistent with those explored in the diffusive limit of the quasiclassical regime²⁷.

In Sec. II, we outline the model Hamiltonian used and we establish the Green's function formalism for calculating the pairing correlations that can inhabit a Weyl semimetal with the possibility of a tilting parameter that can render the WS to a type-II phase. We also discuss the opposite-Pspin and equal-Pspin phonon-mediated electron-electron coupling model that is used to derive the components of the Green's function. We next utilize a quantum mechanical approach to find the supercurrent in a Josephson junction structure comprised of a WS. In Sec. III, we present results for both the pairing correlation symmetries, and the current phase relations for the charge supercurrent. Finally, concluding remarks are given in Sec. IV.

II. METHODS

To model a superconducting WS system, supporting type-I and type-II phases^{26,32}, we use the following Bogoliubov-de Gennes Hamiltonian in the Nambu space:

$$\mathcal{H}(\mathbf{k}) = \begin{pmatrix} H(\mathbf{k}) - \mu\hat{1} & \hat{\Delta} \\ \hat{\Delta}^\dagger & -H^T(-\mathbf{k}) + \mu\hat{1} \end{pmatrix}, \quad (1)$$

in which μ is the chemical potential, \mathbf{k} is the momentum of quasiparticles, $\hat{\Delta}$ is the superconducting gap, and T represents the transpose. The effective Hamiltonian H_{eff} in the low-energy regime, can be then expressed as,

$$H_{\text{eff}} = \int \frac{d\mathbf{k}}{(2\pi)^3} \check{\psi}_{\mathbf{k}}^\dagger \mathcal{H}(\mathbf{k}) \check{\psi}_{\mathbf{k}}, \quad (2)$$

where the associated 1×8 field operator for this Hamiltonian is given by $\check{\psi}_{\mathbf{k}}^\dagger = [\psi_{\mathbf{k}\uparrow}^\dagger, \psi_{-\mathbf{k}\downarrow}^\dagger]$, and $\check{\psi}_{\mathbf{k}} = (\psi_{A\uparrow}^\dagger, \psi_{A\downarrow}^\dagger, \psi_{B\uparrow}^\dagger, \psi_{B\downarrow}^\dagger)$, in which the Pspin (the band degree of freedom) and spin indices are denoted by A, B and \uparrow, \downarrow , respectively.

The diagonal block elements of Eq. (1) are explicitly expressed as:

$$H(\mathbf{k}) = (\beta + \gamma\tau_z)(k_z^2 - Q^2) + \eta(k_x^2 + k_y^2)\tau_z + \alpha_x k_x \tau_x + \alpha_y k_y \tau_y + \alpha_z k_z \tau_z, \quad (3)$$

where the two Weyl points are separated by Q in momentum space. We will consider a broad range of orbital parameters $\alpha_{x,y,z}$, and tilt of the Weyl cones, i.e., β , which is responsible for driving the system into the type-II phase. We will also consider both positive and negative values of the band-structure parameters β and γ , with the latter being responsible for breaking time reversal symmetry and band splitting. Also, a nonzero α_z shifts the Weyl nodes in energies while $\alpha_{x,y}$ can induce a gap at the nodes. The dimension of β, γ, η is $\text{eV} \cdot \text{\AA}^2$ and $\alpha_{x,y,z}$ possess $\text{eV} \cdot \text{\AA}$ unit. Also, the chemical potential that enters the formalism later is in the units of eV and the momenta are scaled using \AA .²⁸⁻³¹

In what follows, we consider a situation where the superconductivity is a consequence of (1) opposite-Pspin and (2) equal-Pspin phonon-mediated mechanism. We also consider a model of opposite-spin electron-electron interactions throughout the paper. The first type of pairing mechanism is characterized by the following two-electron amplitudes:

$$\Delta_{\uparrow\downarrow}^{AB} \langle \psi_{A\uparrow}^\dagger \psi_{B\downarrow}^\dagger \rangle + \text{h.c.} \quad (4)$$

where $\Delta_{\uparrow\downarrow}^{AB}$ is the gap representing BCS spin-singlet phonon mediated electron-electron coupling between the A and B Pspins. The second type of pairing mechanism can be expressed by

$$\Delta_{\uparrow\downarrow}^{AA} \langle \psi_{A\uparrow}^\dagger \psi_{A\downarrow}^\dagger \rangle + \text{h.c.} \quad (5a)$$

$$\Delta_{\uparrow\downarrow}^{BB} \langle \psi_{B\uparrow}^\dagger \psi_{B\downarrow}^\dagger \rangle + \text{h.c.} \quad (5b)$$

where $\Delta_{\uparrow\downarrow}^{AA}$ and $\Delta_{\uparrow\downarrow}^{BB}$ correspond to the gap for BCS spin-singlet phonon mediated electron-electron coupling for each Pspin. In the following, to simplify notation, we suppress the indices so that when applicable, $\Delta_{\uparrow\downarrow}^{AB} \equiv \Delta$ and $\Delta_{\uparrow\downarrow}^{AA} = \Delta_{\uparrow\downarrow}^{BB} \equiv \Delta$.

We next consider the Green's functions for the Weyl semimetal system in the presence of superconductivity. The normal Green's functions g and the anomalous Green's functions f are defined as follows:

$$g_{\rho\rho'}^{\sigma\sigma'}(\tau, \tau'; \mathbf{r}, \mathbf{r}') = -\langle \mathcal{T}_\tau \psi_{\sigma\rho}(\tau, \mathbf{r}) \psi_{\sigma'\rho'}^\dagger(\tau', \mathbf{r}') \rangle, \quad (6a)$$

$$g_{-\rho\rho'}^{\sigma\sigma'}(\tau, \tau'; \mathbf{r}, \mathbf{r}') = -\langle \mathcal{T}_\tau \psi_{\sigma\rho}^\dagger(\tau, \mathbf{r}) \psi_{\sigma'\rho'}(\tau', \mathbf{r}') \rangle, \quad (6b)$$

$$f_{\rho\rho'}^{\sigma\sigma'}(\tau, \tau'; \mathbf{r}, \mathbf{r}') = +\langle \mathcal{T}_\tau \psi_{\sigma\rho}(\tau, \mathbf{r}) \psi_{\sigma'\rho'}(\tau', \mathbf{r}') \rangle, \quad (6c)$$

$$f_{\rho\rho'}^{\sigma\sigma'\dagger}(\tau, \tau'; \mathbf{r}, \mathbf{r}') = +\langle \mathcal{T}_\tau \psi_{\sigma\rho}^\dagger(\tau, \mathbf{r}) \psi_{\sigma'\rho'}^\dagger(\tau', \mathbf{r}') \rangle, \quad (6d)$$

where \mathcal{T}_τ is the time ordering operator, and τ, τ' are the imaginary times. Here, ρ, ρ' and σ, σ' denote the spin and Pspin indices and $\langle \dots \rangle$ denotes thermodynamic averaging. In particle-hole space, the Green's function satisfies,

$$\begin{pmatrix} \hat{H}(\mathbf{r}) - i\omega_n & \hat{\Delta}(\mathbf{r}) \\ \hat{\Delta}^*(\mathbf{r}) & \mathcal{T}_t \hat{H}(\mathbf{r}) \mathcal{T}_t^\dagger + i\omega_n \end{pmatrix} \check{g}(i\omega_n; \mathbf{r}, \mathbf{r}') = \delta(\mathbf{r} - \mathbf{r}'), \quad (7)$$

in which $\omega_n = \pi(2n+1)k_B T$ is the Matsubara frequency, $n \in \mathbb{Z}$, k_B is the Boltzman constant, T is temperature, \mathcal{T}_t is the time reversal operator, and $\hat{\Delta}(\mathbf{r})$ is the superconducting gap in real space. Note that the Hamiltonian in real space $\hat{H}(\mathbf{r})$ is obtained by replacing $i\mathbf{k} \equiv (\partial_x, \partial_y, \partial_z)$ in $H(\mathbf{k})$, in Eq. (3). The matrix form of the Green's function reads:

$$\check{g}(i\omega_n; \mathbf{r}, \mathbf{r}') = \begin{pmatrix} \hat{g}(i\omega_n; \mathbf{r}, \mathbf{r}') & \hat{f}(i\omega_n; \mathbf{r}, \mathbf{r}') \\ \hat{f}^\dagger(i\omega_n; \mathbf{r}, \mathbf{r}') & \hat{g}(i\omega_n; \mathbf{r}, \mathbf{r}') \end{pmatrix}, \quad (8)$$

where we denote the 4×4 matrices by the symbol, $\hat{\dots}$, and 8×8 matrices by the symbol, $\check{\dots}$.

In order to calculate the supercurrent flowing through a Weyl semimetal Josephson junction, we assume a steady state situation where the charge density ρ in the system is constant in time, namely $\partial\rho/\partial t \equiv 0$. To ultimately calculate the charge current density, we employ the quantum mechanical definition

of the time-evolution of ρ for a generic system that ensures charge conservation in the steady state, namely:

$$\frac{\partial\rho}{\partial t} = \lim_{\mathbf{r} \rightarrow \mathbf{r}'} \sum_{\sigma\rho\nu\sigma'\rho'\nu'} \frac{1}{i\hbar} \left[\psi_{\sigma\rho\nu}^\dagger(\mathbf{r}') \mathcal{H}_{\sigma\rho\nu\sigma'\rho'\nu'}(\mathbf{r}) \psi_{\sigma'\rho'\nu'}(\mathbf{r}) - \psi_{\sigma\rho\nu}^\dagger(\mathbf{r}') \mathcal{H}_{\sigma\rho\nu\sigma'\rho'\nu'}^\dagger(\mathbf{r}') \psi_{\sigma'\rho'\nu'}(\mathbf{r}') \right]. \quad (9)$$

Here $\mathcal{H}_{\sigma\rho\nu\sigma'\rho'\nu'}$ is the component form of Eq. (1) with the Pspin, spin, and particle-hole (ν, ν') indices written explicitly. We now use the law of current conservation to arrive at the following quantum mechanical expression for the current density:

$$\mathbf{J} = \int d\mathbf{r} \{ \hat{\psi}^\dagger(\mathbf{r}) \vec{\mathcal{H}}(\mathbf{r}) \hat{\psi}(\mathbf{r}) - \hat{\psi}^\dagger(\mathbf{r}) \overleftarrow{\mathcal{H}}(\mathbf{r}) \hat{\psi}(\mathbf{r}) \}, \quad (10)$$

where $\mathcal{H}(\mathbf{r})$ is given by Eq. (1), after the substitution $i\mathbf{k} \equiv (\partial_x, \partial_y, \partial_z)$. The arrows point to the specific wavefunctions that are acted on by the derivative operators in the Hamiltonian. Note that any property of the system (including anisotropy and inhomogeneity) are indeed imbedded within the Hamiltonian of the system, associated wavefunctions, and boundary conditions (see below for more details).

III. RESULTS AND DISCUSSIONS

In this section we present results that depict representative behavior of the pair correlation profiles that may evolve in Weyl semimetal systems. We examine the momentum-space profiles and show that by varying experimentally relevant parameters, the effective symmetry classes of the superconducting correlations can undergo significant transformations. To compliment this, the charge supercurrent flow is then studied in a ballistic SNS Josephson structure, where a phase difference between the two superconducting electrodes is established. The direction and periodicity of supercurrent flow, and the possible emergence of $0-\pi$ transitions are investigated as a function of orbital effects, as well as tilt and spacing of the Weyl cones.

A. Symmetry profile of superconducting pair correlations

Here we present the anomalous Green's function $\hat{f}(i\omega; \mathbf{k})$ and explore different symmetries that may arise by manipulating the Weyl semimetal material parameters. In the calculations that follow, we consider a representative node separation corresponding to $Q = 0.4\pi$, and note that our conclusions are independent of this specific choice. For simplicity, we consider the zeroth mode of the Matsubara frequency, following the fact that parity is not affected by the frequency domain. Each component of $\hat{f}(i\omega; \mathbf{k})$ describes a specific pairing correlation function. To further simplify our calculations, we consider a system that is invariant in all directions so that the momenta $k_{x,y,z}$ are good quantum numbers and can be treated algebraically in momentum space. By solving Eq. (7) in conjunction with the opposite-Pspin phonon mediated coupling

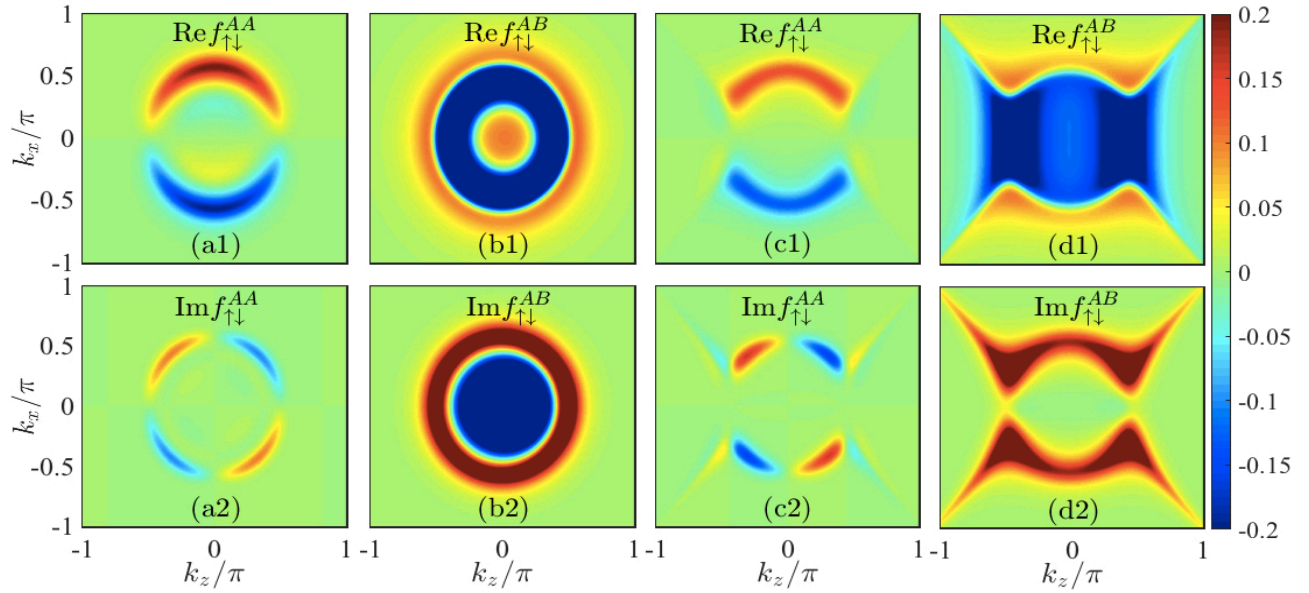


FIG. 1. (Color online). Real and imaginary parts of the superconducting correlations for the *opposite*-pseudospin phonon mediated electron-electron interaction plotted as a function of momenta k_x and k_z . For illustrative purposes, the momentum component k_y is set to zero. The following pair correlations are shown: $f_{\uparrow\downarrow}^{AA}$ and $f_{\uparrow\downarrow}^{AB}$. (a)-(b) ($\gamma > \beta$) We use the representative parameters $\gamma = 1.3$, $\beta = 0.1$, $\alpha_z = \alpha_{xy} = 0.2$, $\mu = 0.5$, $\eta = 1$, and $Q = 0.4\pi$. (c)-(d) ($\gamma < \beta$) We use the representative parameters $\gamma = 0.1$, $\beta = 1.3$, $\alpha_z = \alpha_{xy} = 0.2$, $\mu = 0.5$, $\eta = 1$, and $Q = 0.4\pi$.

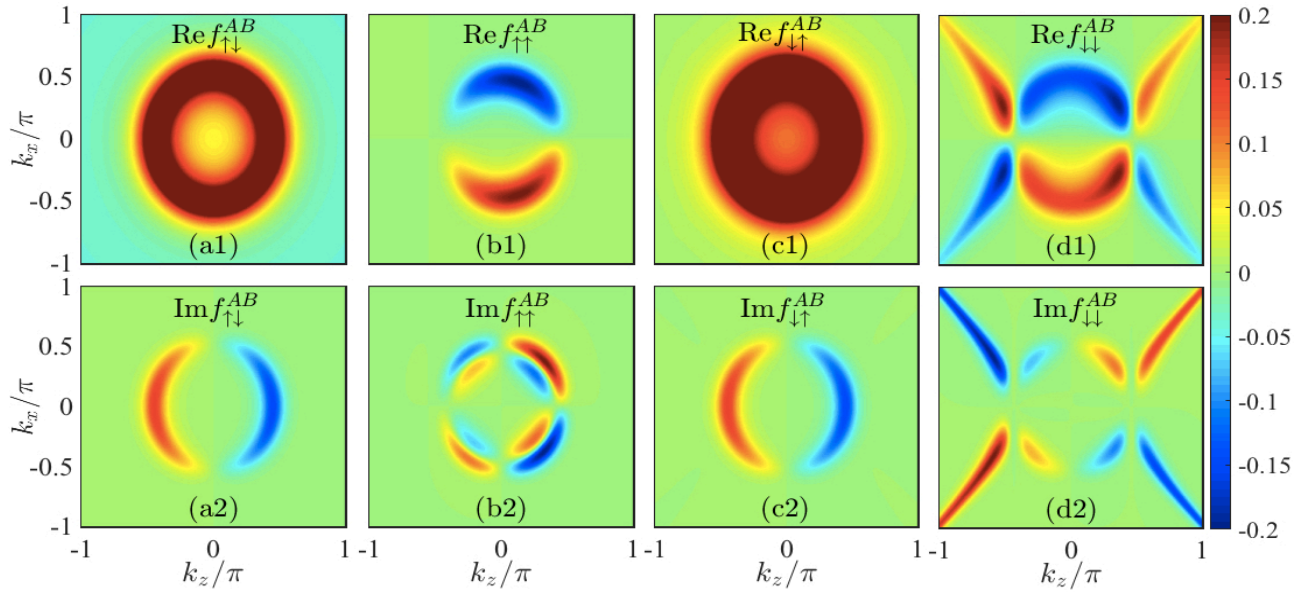


FIG. 2. (Color online). Real and imaginary parts of the superconducting correlations for the *equal*-pseudospin phonon mediated electron-electron interaction plotted as a function of momenta k_x and k_z . The following pair correlations are shown: $f_{\uparrow\downarrow}^{AA}$ and $f_{\uparrow\downarrow}^{AB}$. The parameters here are the same as in Fig. 1.

of Eq. (4), we end up with the following expressions for the

superconducting correlations:

$$f_{\uparrow\uparrow}^{AA} = 0 \quad (11a)$$

$$f_{\uparrow\downarrow}^{AA} = \frac{2}{\mathcal{D}} \alpha_{xy} \Delta \underbrace{(k_x - ik_y)}_{p_-} \underbrace{(\Lambda + \mu + \Omega(\gamma - \beta))}_{\mathcal{D}_-}, \quad (11b)$$

$$f_{\uparrow\uparrow}^{AB} = 0 \quad (11c)$$

$$f_{\uparrow\downarrow}^{AB} = -\frac{\Delta}{\mathcal{D}} [-(\Omega(\gamma - \beta) + \Lambda + i\omega_n) (\Omega(\beta + \gamma) + \Lambda + i\omega_n) + \Delta^2 + \alpha_{xy}^2 (k_x^2 + k_y^2) + \alpha_z^2 k_z^2 + 2\alpha_z k_z (\mu - \beta\Omega) - 2\mu\beta\Omega], \quad (11d)$$

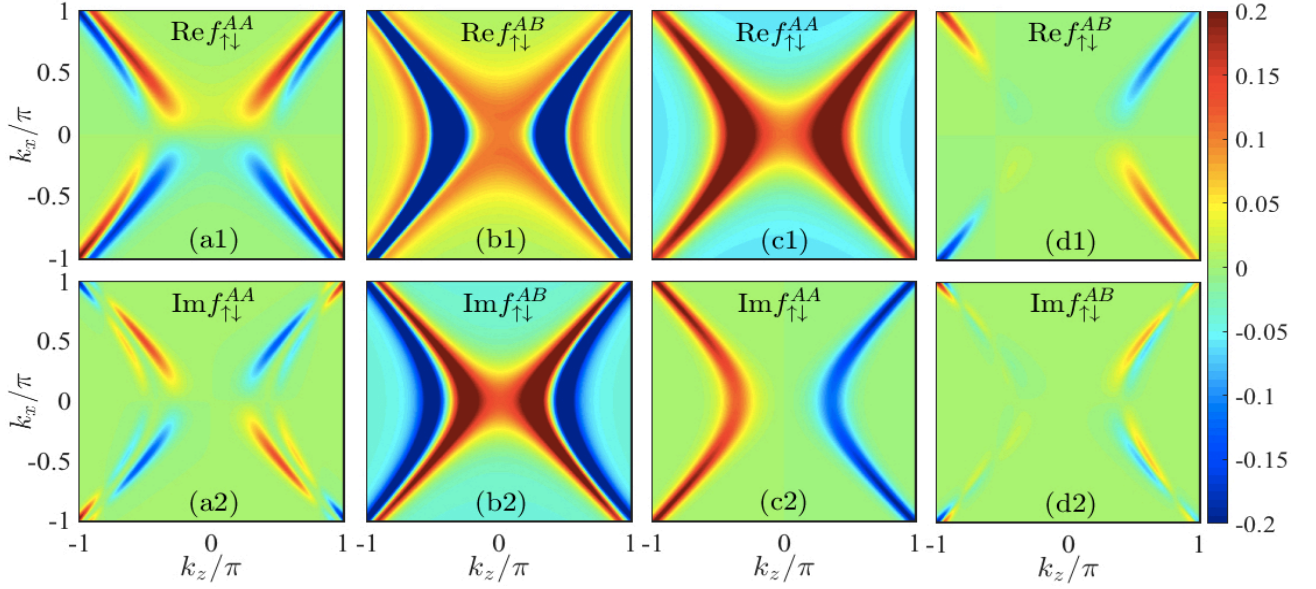


FIG. 3. (Color online). Real and imaginary parts of the superconducting correlations $f_{\uparrow\downarrow}^{AA}$ and $f_{\uparrow\downarrow}^{AB}$ plotted as a function of momenta k_x and k_z . (a)-(b) The *opposite*-pseudospin phonon mediated electron-electron interaction is considered and parameters are identical to those of Figs. 1(a)-1(b) except we now set $\gamma = -1.3$. (c)-(d) The *equal*-pseudospin phonon mediated electron-electron interaction is set and parameters are identical to those of Figs. 2(a)-2(b), except now we flip the sign of γ to minus $\gamma = -1.3$.

in which \mathcal{D} is given by:

$$\begin{aligned} \mathcal{D} = & (k_x^2 + k_y^2)\alpha_{xy}^2(-\mu^2 + (k_x^2 + k_y^2)\alpha_{xy}^2 + \Delta^2 + 2\mu(\beta\Omega - i\omega_n) + (k_z\alpha_z + \Lambda + (\beta + \gamma)\Omega - i\omega_n)(k_z\alpha_z + \Lambda - \beta\Omega + \gamma\Omega + i\omega_n)) + \\ & \Delta^2((k_x^2 + k_y^2)\alpha_{xy}^2 + \Delta^2 - (\mu + k_z\alpha_z + \Lambda - \beta\Omega + \gamma\Omega + i\omega_n)(-\mu - k_z\alpha_z + \Lambda + (\beta + \gamma)\Omega + i\omega_n)) + \\ & (\Delta^2(-\mu + k_z\alpha_z + \Lambda + (\beta + \gamma)\Omega - i\omega_n) + (\mu^2 - (k_x^2 + k_y^2)\alpha_{xy}^2 - (k_z\alpha_z + \Lambda + (\beta + \gamma)\Omega - i\omega_n)(k_z\alpha_z + \Lambda - \beta\Omega + \gamma\Omega + i\omega_n)) + \\ & \mu(-2\beta\Omega + 2i\omega_n))(-\mu - k_z\alpha_z + \Lambda + (\beta + \gamma)\Omega + i\omega_n)(-\mu + k_z\alpha_z - \Lambda + \beta\Omega - \gamma\Omega + i\omega_n) \end{aligned} \quad (12)$$

where we have defined $\Omega = k_z^2 - Q^2$, and $\Lambda = \eta(k_x^2 + k_y^2)$. In a similar fashion, and using the symmetry relations appropriate for the Green's function components, one can obtain the other components of $\hat{f}(i\omega; \mathbf{k})$. We have derived all components of $\hat{g}(i\omega; \mathbf{k})$, however for the purposes shown in this work, the components presented above are adequate.

Here, we have set $\alpha_x = \alpha_y = \alpha_{xy}$ to further simplify our expressions. Note that if we set $\alpha_{xy} = 0$, Eq. (12) reduces to,

$$\mathcal{D} = -\Delta^2 + (-\mu + k_z\alpha_z - \Lambda + \beta\Omega - \gamma\Omega + i\omega_n) \quad (13)$$

$$(\mu - k_z\alpha_z - \Lambda - (\beta + \gamma)\Omega + i\omega_n), \quad (14)$$

and we also find,

$$f_{\uparrow\uparrow}^{AA} = 0, \quad (15a)$$

$$f_{\uparrow\downarrow}^{AA} = 0, \quad (15b)$$

$$f_{\uparrow\uparrow}^{AB} = 0, \quad (15c)$$

$$f_{\uparrow\downarrow}^{AB} = \frac{\Delta}{\mathcal{D}}. \quad (15d)$$

As seen, the orbital term is indeed responsible for inducing equal-Pspin pair correlations in WS so that $f_{\uparrow\downarrow}^{AA}$ is directly proportional to α_{xy} . The expression governing the equal-Pspin component of the anomalous Green's function (when

$\alpha_{xy} \neq 0$) in Eq. (11b) has several important features: The numerator is proportional to $\mathcal{P}_- = k_x - ik_y$, which is of odd-parity, and corresponds to an effective *p*-wave symmetry ($p_x - ip_y$). The second term in parentheses, \mathcal{D}_- , containing Ω and Λ , is of even-parity and has a symmetry expressible in the form $|a|(k_x^2 + k_y^2) \pm |b|k_z^2$, where a and b are coefficients that depend on η , γ , and β . Specifically, from \mathcal{D}_+ , we find that $a \equiv \eta$ and $b \equiv (\gamma - \beta)$. Hence, depending on the choice of parameters (for example, in the regime where $\beta > \gamma$ or $\beta < \gamma$), the symmetry classification for the second term can be of the *s*-wave ($|a|(k_x^2 + k_y^2) + |b|k_z^2$) or *d*-wave ($|a|(k_x^2 + k_y^2) - |b|k_z^2$) types. Depending on the symmetry of \mathcal{D}_- , the numerator of Eq. (11b) belongs to the *p*-wave or *f*-wave symmetry classes. The complete symmetry profiles of $f_{\uparrow\downarrow}^{AA, BB}$ depend also on the symmetry of the denominator \mathcal{D} . Therefore, in what follows, we study *effective* symmetries of the superconducting pair correlations. Upon variations of the parameters η , γ , and β in Eqs. (11b) and (11d), it is evident that the cumulative effect on $f_{\uparrow\downarrow}^{AA}$ and $f_{\uparrow\downarrow}^{AB}$ is to produce a spatial symmetry that can be classified as effectively *p*-wave and *f*-wave. Although \mathcal{D} can have an effective *s*-wave symmetry, depending on η , γ , β , if α_z is nonzero, the overall symmetry of $f_{\uparrow\downarrow}^{AA}$ and $f_{\uparrow\downarrow}^{AB}$ can change as seen in Eqs. (12) and (13). Although more lengthy,

an analysis of the components $f_{\uparrow\downarrow}^{BB}$, and $f_{\uparrow\downarrow}^{BA}$ reveals similar possibilities. For instance, if we set $\alpha_z = 0$, we see that the numerators of $f_{\uparrow\downarrow}^{BA}$ can show either s -wave or d -wave effective symmetries, depending again, on the parameters η , γ , and β . Thus, for the phonon mediated unequal-Pspin scenario, the superconducting pairing correlations can change their effective spatial symmetry profiles from one symmetry class to another, simply by manipulating the material parameters of a Weyl semimetal. As recently demonstrated, control of these parameters is possible by, for example, applying strain to the system.²⁸⁻³¹ Also, unconventional pairings and their symmetries were recently studied in systems with and without the lack of inversion symmetry.⁷⁴⁻⁷⁶ It is also worth noting that our results above illustrate that superconducting Weyl semimetals can develop odd-frequency symmetries.⁷³

To further shed light on the symmetry profiles of these superconducting correlations, in Figs. 1-3, we present a few representative profiles for the real and imaginary parts of the equal-Pspin and opposite-Pspin components as a function of the momenta k_x and k_y . The upper row of panels corresponds to the real parts, while the bottom row is for the imaginary parts. For simplicity, we consider zero momentum along y , $k_y = 0$. We also consider here two regimes ($\beta < \gamma$ and $\beta > \gamma$) and equal strengths of the orbital parameters: $\alpha_z = \alpha_{xy} = 0.2$. In Figs. 1(a)-1(b) we implement a representative set of parameters: $\gamma = 1.3$, $\beta = 0.1$, $\mu = 0.5$, $\eta = 1$, and $Q = 0.4\pi$. As seen in Figs. 1(b1) and 1(b2), the *effective* symmetry of the $f_{\uparrow\downarrow}^{AB}$ correlations are of the s -wave type, which is indeed fully consistent with our discussion of Eq. (11d). Likewise, Figs. 1(a1) and 1(a2) show that the effective symmetry of both imaginary and real parts of $f_{\uparrow\downarrow}^{AA}$ are of the p -wave type, consistent with Eqs. (11b). We note that here we consider the regime where $\gamma > \beta$.

In order to illustrate how the effective d -wave and f -wave symmetries might evolve, we now set $\gamma = 0.1$ and $\beta = 1.3$, corresponding to the $\gamma < \beta$ regime. Note that, according to

$$\begin{aligned} \mathcal{D} = & -(-k_x + ik_y)\alpha_{xy}((k_x - ik_y)\alpha_{xy}\Delta^2 + (k_x + ik_y)\alpha_{xy}(-\mu^2 + (k_x^2 + k_y^2)\alpha_{xy}^2 + 2\mu(\beta\Omega - i\omega_n) + (k_z\alpha_z + \Lambda + (\beta + \gamma)\Omega - i\omega_n) \\ & (k_z\alpha_z + \Lambda - \beta\Omega + \gamma\Omega + i\omega_n))) + \Delta^2((k_x + ik_y)^2\alpha_{xy}^2 + \Delta^2 + (-\mu + \Lambda + (\beta + \gamma)\Omega)^2 - (k_z\alpha_z - i\omega_n)^2) + \\ & (-\Delta^2(\mu + k_z\alpha_z + \Lambda - \beta\Omega + \gamma\Omega + i\omega_n) + (\mu^2 - (k_x^2 + k_y^2)\alpha_{xy}^2 - (k_z\alpha_z + \Lambda + (\beta + \gamma)\Omega - i\omega_n) \\ & (k_z\alpha_z + \Lambda - \beta\Omega + \gamma\Omega + i\omega_n) + \mu(-2\beta\Omega + 2i\omega_n))(-\mu - k_z\alpha_z + \Lambda + (\beta + \gamma)\Omega + i\omega_n))(-\mu + k_z\alpha_z - \Lambda + \beta\Omega - \gamma\Omega + i\omega_n)). \end{aligned} \quad (17)$$

We see that this kind of pairing interaction results in complicated expressions for the superconducting correlations, specifically for the denominator. Therefore, we evaluate them numerically in Fig. 2. Similar to the previous case, if we set $\alpha_{xy} = 0$, the expressions simplify considerably:

$$f_{\uparrow\uparrow}^{AA} = 0, \quad (18a)$$

$$f_{\uparrow\downarrow}^{AA} = \frac{\Delta}{\mathcal{D}}, \quad (18b)$$

$$f_{\uparrow\uparrow}^{AB} = 0, \quad (18c)$$

$$f_{\uparrow\downarrow}^{AB} = 0, \quad (18d)$$

the discussion above, one is able to achieve similar symmetry changes in the effective symmetry profiles (described below) by tuning and/or reversing the sign of the parameters γ , η , and β . The resultant superconducting correlations are shown in Figs. 1(c)-1(d). We clearly observe in Figs. 1(b1), 1(b2), 1(d1), and 1(d2) that the previous effective s -wave symmetry has transformed into an effective d -wave class. Likewise, Figs. 1(a1), 1(a2), 1(c1), and 1(c2) illustrate that the previous effective p -wave symmetry has become of the f -wave type, which arises from the multiplication of terms with effective p -wave and d -wave symmetries, as discussed in connection with Eqs. (11b) and (11d). As for the effects of increasing the tilt parameter β , Eqs. (11) reveal that there are two competing effects that determine the final symmetry of the pair correlations: As β increases, the pair correlations involving the term $(\gamma - \beta)$ decrease their s -wave character [$|a|(k_x^2 + k_y^2) + |b|k_z^2$], which is countered by the parameter γ and drives the correlations into a d -wave symmetry class [$|a|(k_x^2 + k_y^2) - |b|k_z^2$]. Thus, a multitude of possibilities arise for the pair correlation symmetries depending on the material properties and whether the Weyl semimetal is type-I or type-II.

To gain additional insight, we have also calculated the superconducting pairing correlations starting from an equal-Pspin scenario given by Eq. (5). After performing the calculations, we find the following expressions for the components of anomalous Green's function:

$$f_{\uparrow\uparrow}^{AA} = 0, \quad (16a)$$

$$f_{\uparrow\downarrow}^{AA} = \frac{1}{\mathcal{D}}[\Delta((k_x - ik_y)^2\alpha_{xy}^2 + \Delta^2 + (\mu + \Lambda + (-\beta + \gamma)\Omega)^2 - (k_z\alpha_z + i\omega_n)^2)], \quad (16b)$$

$$f_{\uparrow\uparrow}^{AB} = 0, \quad (16c)$$

$$f_{\uparrow\downarrow}^{AB} = -\frac{1}{\mathcal{D}}[2\alpha_{xy}\Delta(k_x(\mu + k_z\alpha_z - \beta\Omega) + ik_y(\Lambda + \gamma\Omega + i\omega_n))], \quad (16d)$$

$$\mathcal{D} = \Delta^2 + (-\mu + \Lambda + (\beta + \gamma)\Omega)^2 - (k_z\alpha_z - i\omega_n)^2. \quad (19)$$

In agreement with our initial assumption for the electron-electron interactions [i.e., Eq. (5)], we find that $f_{\uparrow\downarrow}^{AA}$ (or equivalently $f_{\uparrow\downarrow}^{BB}$) is the only nonzero component with even-parity when $\alpha_z = 0$, which is evidently of the s -wave type. In Fig. 2, we have plotted the equal-Pspin and opposite-Pspin components of Green's function as a function of k_x , k_z , where $k_y = 0$. The parameters set are identical to that used in Fig. 1. As seen in Figs. 2(a)-2(b) and 2(c)-2(d), when we move from the $\gamma > \beta$ regime to the regime where $\gamma < \beta$, only $f_{\uparrow\downarrow}^{AB}$ shows a discernible change in its spatial symmetry, while $f_{\uparrow\downarrow}^{AA}$ remains almost entirely intact. This is in contrast to the previous cases

where both components $f_{\uparrow\downarrow}^{AB}$ and $f_{\uparrow\downarrow}^{AA}$ show changes in their symmetries. Nevertheless, we can conclude that the symmetry change is robust and can occur for the two electron-electron interaction scenarios considered in this paper (see also the following discussions).

Figure 3 illustrates the pairing correlations $f_{\uparrow\downarrow}^{AB}$ and $f_{\uparrow\downarrow}^{AA}$, where we have simply flipped the sign of $\gamma = -1.3$, and kept $\beta = 0.1$ unchanged. In Figs. 3(a)-3(b), we plot the correlations for when the interaction between electrons with opposite spins are of the opposite-Pspins [Eq. (4)]. In contrast, Figs. 3(c)-3(d) correspond to equal-Pspin opposite-spin electron-electron interactions. It can be seen that by flipping the sign of γ , one can achieve pronounced symmetry changes in the superconducting correlations. The same feature can be observed when the sign of β is reversed in the opposite regime where $\beta > \gamma$ (not shown).

Note that the possibility of symmetry change in spatial profiles of pair correlations relies on a sign change of the momenta coefficients. Such situations can be precisely determined by first-principles calculations; e.g., when the system experiences external strain or is subject to doping and intercalation. A practical example is when a black phosphorus monolayer is under the application of an external strain, as was recently discussed²⁸⁻³¹. The band-structure parameters were obtained using density-functional-theory computations, and symmetry calculations demonstrated that the momenta coefficients can change sign depending on the strength and direction of the applied in-plane strain. Hence, angular point-contact tunneling spectroscopy experiments or Meissner effect imaging are ideal probes to confirm the symmetry-change predictions discussed above.

An important phenomenon that can be additionally accounted for in our calculations and serve as a controlling parameter, is an exchange field^{28,29}. Although we have not explicitly written it in our formulations, to incorporate an exchange field with three nonzero components h_i , the terms $h_x\rho_x + h_y\rho_y + h_z\rho_z$ should be attached to each Pspin [see Refs. 28-31], in which ρ_i are Pauli matrices in spin space. We have investigated the superconducting pair correlations when the exchange field is nonzero in different directions. Our results (not shown) illustrate that the change of symmetry classes predicted above occurs for the spin-triplet superconducting correlations as well in the presence of an exchange field.

Our theoretical methods may also be extended to a scenario similar to the one investigated in a recent experiment that observed controlled superconductivity in MoTe₂ by the application of an external mechanical strain⁶⁵. It was observed that by the application of strain to MoTe₂, the superconducting critical temperature T_c increased. In consideration of this, it would be of interest to study T_c for WS systems over a broad range of material and geometrical parameters. In this case, the superconducting gap function should be solved self-consistently to extract T_c , which is however, a nontrivial and formidable task that is postponed for future works.^{80,81}

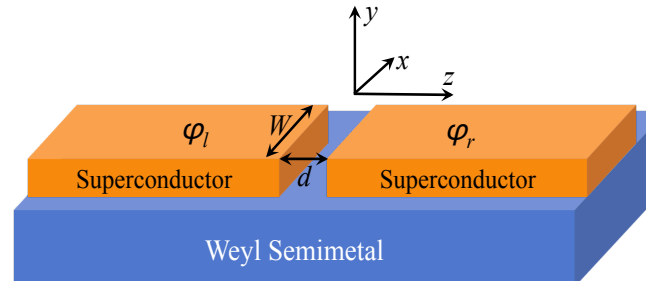


FIG. 4. (Color online). Schematic of a Weyl semimetal Josephson junction. The junction interfaces lie in the xy plane, with the normal to the interfaces along the z direction. The interfaces between the normal state Weyl semimetal and the superconductors are located at $z = \pm d/2$. The width of the junction is W and the macroscopic phase of the left and right superconductors are labeled by φ_l and φ_r , respectively.

B. Charge Supercurrent

We now proceed to investigate the supercurrent flow through a Weyl Josephson junction. We consider a SNS type structure with a phase difference $\varphi = \varphi_l - \varphi_r$ established between the two superconducting electrodes [see Fig. 4]. To compute the total charge current, we take the current density perpendicular to the interface, which is in our case J_z , and integrate over the x direction, i.e., $I(\varphi) = \int_0^W dx J_z(x, z, \varphi)$. Note that the current is independent of the z -coordinate as required by charge conservation. Upon diagonalizing $\mathcal{H}(\mathbf{r})$, we calculate the spinors $\psi_{\sigma\rho\nu}$ within each region. Next, in order to obtain appropriate wavefunction in the normal region of the Josephson configuration, we match wavefunctions at the left $\hat{\psi}_l(z = -d/2) = \hat{\psi}_r(z = -d/2)$ and right boundaries $\hat{\psi}_r(z = +d/2) = \hat{\psi}_l(z = +d/2)$, and apply the continuity condition $\partial_{\mathbf{k}}\mathcal{H}_l(\mathbf{k})\hat{\psi}_l = \partial_{\mathbf{k}}\mathcal{H}_r(\mathbf{k})\hat{\psi}_r$, at the left and right superconductor interfaces. At the left boundary, \mathcal{H}_l and \mathcal{H}_r correspond to the Hamiltonians of the superconducting and normal regions ($\hat{\psi}_l$ and $\hat{\psi}_r$ are their associated wavefunctions), respectively, whereas at the right boundary they represent the Hamiltonians of the normal and superconducting regions, respectively. We note that, in order to accommodate a wide range of parameters without missing the important physics, we make no assumptions and approximations regarding the strength of the parameters involved that would normally simplify the wavefunctions. For example, the quasi-classical approximation assumes that μ is largest energy in the system, which considerably simplifies the wavefunctions, but at the cost of losing important information for regimes where μ is small²⁶⁻²⁹. The resultant analytic expressions involving 1×8 spinors are therefore very cumbersome, and we omit the explicit expressions, presenting numerical results only when evaluating observable quantities. The junction length is fixed at a finite representative value ($d \approx 7.5$ nm), and we assume that the junction width W is sufficiently large ($W \approx 100$ nm) so that boundary effects along the width direction are negligible. The central junction segment is undoped with $\mu_N = 0$,

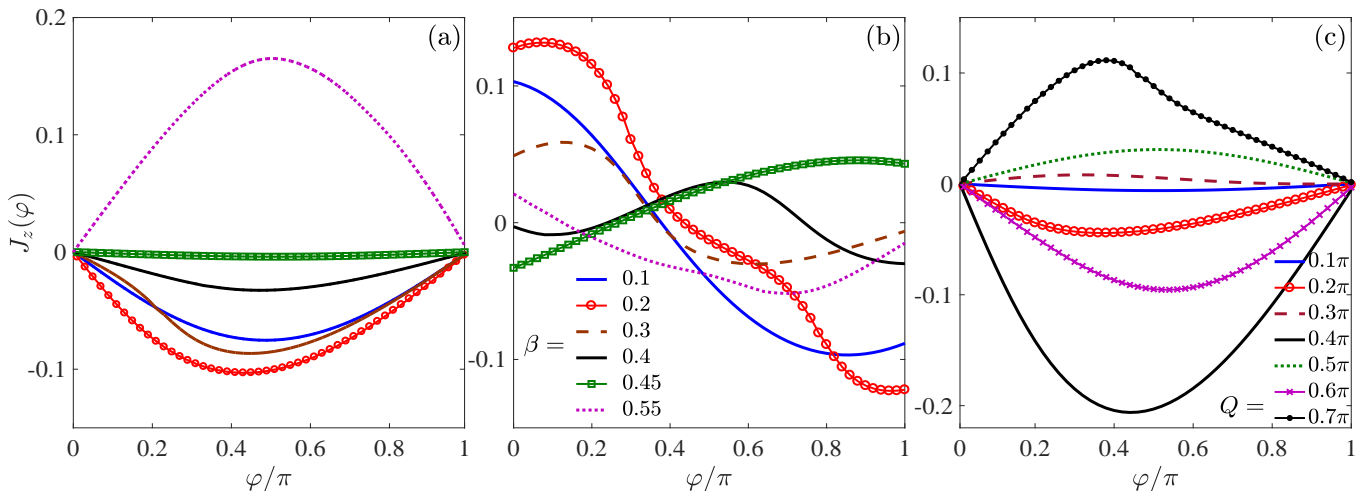


FIG. 5. (Color online). Current density flowing in the z direction, $J_z(\varphi)$, as a function of superconducting phase difference φ applied across the junction for various values of the tilting parameter β and separation of Weyl nodes Q (see legends). In (a) the orbital term α_z is set zero. In (b) the orbital term α_z possesses a representative finite value of 0.2. In (c) we set α_z zero and vary Q . The other parameters are set as follows: $\gamma = 0.5, \beta = 0.2, \alpha_{x,y} = 1$, and $\eta = 1$.

while the chemical potential in the superconducting segments have the representative value $\mu_S = 0.4$. It is assumed that superconductivity is induced into the Weyl semimetal by virtue of proximity effects. From the component of the current density normal to the interfaces, J_z , the charge current flowing through the junction corresponds to $2eJ_z|\Delta|W/\hbar$. As seen from the components of the Hamiltonian in Eq. (3), the conical tilting parameter β and the inversion symmetry breaking terms α_{xy}, α_z are expected to strongly influence the flow of charge through the junction.

We show in Fig. 5, the supercurrent density J_z as a function of φ for a moderate range of the Weyl cone tilting parameter β (see legend). Two different anisotropic states are considered: (a) where the orbital term vanishes $\alpha_z = 0$, and (b) $\alpha_z = 0.2$. When the orbital term is set to zero, we see in Fig. 5(a) that the supercurrent profile has the conventional sinusoidal 2π periodicity. Increasing the tilt of the Weyl cones is shown to cause a non-monotonic variation in the amplitudes. Indeed, by tuning β appropriately, the current can almost vanish or change direction altogether. Note that the current-phase periodicity changes to 4π by the presence of higher harmonics at the current reversal points^{28,29}. The appearance of higher order harmonics in the current-phase-relation can be made more pronounced by manipulating the WS parameter set (not shown). Next, in Fig. 5(b) the inversion symmetry breaking term takes a representative value corresponding to $\alpha_z = 0.2$. By introducing a z -component to the inversion symmetry breaking term, the current-phase-relation undergoes a phase shift leading to a nonvanishing current at $\varphi = 0, \pi$, creating a φ_0 -state. Our results are consistent with recent findings in quasiclassical Weyl semimetal systems containing disorder²⁷. Within a quasiclassical approach, it was found that supercurrent can flow through a triplet channel, and the φ_0 state is independent of the diffusion constant, demonstrating that this self-biased current can occur regardless of the density of nonmagnetic

impurities and disorder in WS systems. Hence, the predicted robust self-biased current should be experimentally accessible over a wide range of parameters.^{27,28,77–79,82,83} It is worth mentioning that in a recent experiment,⁸³ this self-biased current was observed using a Bi_2Se_3 platform, which is in agreement with theoretical predictions for topological insulator Josephson junctions^{77–79}.

We also see that for type-II Weyl semimetals, increases in the conical tilt leads to a nontrivial current density that is accompanied by the appearance of additional harmonics. In Fig. 5(c), we investigate the effects of varying the Weyl node separation parameter Q . Here we set $\alpha_z = 0$, and $\beta = 0.2$. We clearly see that this parameter can also control the direction and magnitude of the supercurrent, as well as the appearance of higher harmonics. In addition, the junction thickness d can be exploited for controlling these phenomena in the supercurrent (not shown). Hence, our results demonstrate that a Josephson junction made of a type-I or type-II Weyl semimetal offers experimentally accessible parameters that can essentially act as control knobs to tune the supercurrent behavior. In many instances, these parameters are externally controllable, e.g., by applying an external strain^{28,29}. For the exhibited sign reversals, manifestation of higher harmonics, and induction of a φ_0 state in the supercurrents shown above, no exchange interaction or Zeeman field was involved. This is in contrast to previously proposed platforms where the exchange field is an essential ingredient, and which might complicate experimental situations.

An experimentally relevant quantity is the critical supercurrent (maximum of the charge supercurrent defined by $\max(|J_z(\varphi)|)$) that can vary when one of the junction parameters changes. The generic behaviour of the critical supercurrent in the Weyl semimetal Josephson junction we considered can be inferred from Fig. 5. For example, from Fig. 5(a) it is clear that the critical current in such a junction oscillates as a

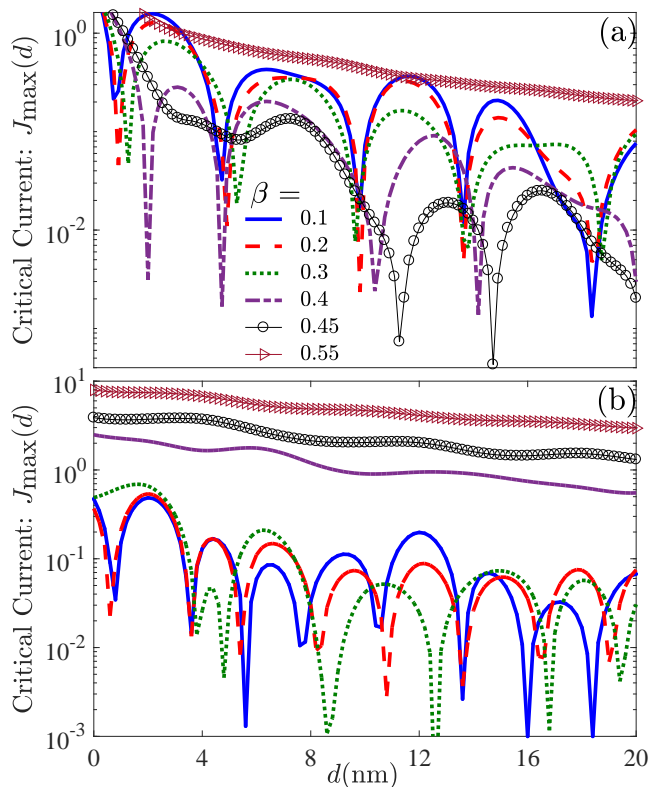


FIG. 6. (Color online). Critical charge current density J_{\max} flowing across the Josephson junction shown in Fig. 5 as a function of junction thickness d . In (a) we set $Q = 0.4\pi$ and (b) $Q = 0.7\pi$ and show the influence of the tilting parameter β on the critical supercurrent. The rest of junction's parameters are set as follows: $\gamma = 0.5$, $\alpha_{x,y} = 1$, $\alpha_z = 0$, and $\eta = 1$.

function of β . The behaviour of the critical current can similarly be seen by considering other parameters, such as Q (in Fig. 5(c)). These findings are summarized in the critical current plots shown in Fig. 6. In order to be consistent with the current phase relations presented in Fig. 5, we use identical parameters in Fig. 6. In Fig. 6(a) we set $Q = 0.4\pi$ and in 6(b) $Q = 0.7\pi$. The critical supercurrent is shown as a function of junction thickness d for various values of the tilting parameter $\beta = 0.1, 0.2, 0.3, 0.4, 0.45, 0.55$. We see that the supercurrent undergoes multiple $0-\pi$ reversals by varying the junction thickness. Depending on Q and the value for γ , increasing the tilting parameter beyond a threshold value causes the critical supercurrent to change its behaviour drastically, as it reduces to a simple decaying function. This behaviour is originated from the now dominated tilting parameter, which is consistent with Ref.²⁷. Increasing β results in amplifying the magnitude of critical supercurrent. It is worth mentioning that we have purposefully chosen the orientation of the junction length to be along the z direction. Because the Hamiltonian in Eq. (1) is not isotropic, the most interesting features of current transport in the model Weyl semimetal we consider appears when the current flows in the z direction. The behavior follows from

the interplay of broken time reversal and inversion symmetries in this specific direction. From Eq. (1), it is apparent that the interesting phenomena presented in Fig. 5 are absent when the Josephson junction is directed either along x or y , so that the SN and NS interfaces are oriented along z (y or x orientations, respectively). In particular, the appearance of the φ_0 self-biased Josephson state is specific to the charge current component flowing in the z direction in our model Hamiltonian [Eq. (1)]. Lastly, it is worth mentioning that recent experiments on Cd_3As_2 semimetal Josephson junctions have found 4π periodic current phase relations^{84,85}. This 4π periodic current phase relation is attributed to the presence of topological superconductivity. Note that a 4π periodic current phase relation can also appear in a ballistic Josephson junction made of surface states of a three-dimensional topological insulator, and persist even in the quasiclassical regime where the chemical potential is large compared to other energy scales⁷⁹.

IV. CONCLUSIONS

Starting from equal-pseudospin and unequal-pseudospin phonon mediated spin-singlet electron pair couplings, we have studied the effective superconducting correlations that can exist in a Weyl semimetal system with the possible tilting of the Weyl cones, rendering the WS into type-II phase. We have considered a situation where the quasiparticle momenta are good quantum numbers, and derived the components of the Green's function that allow us to investigate the effective symmetry profiles of various superconducting correlations. Our results demonstrate that by properly engineering a Weyl semimetal system using intrinsic, and externally controllable parameters, the superconducting correlations can change symmetries from effective s -wave and p -wave classes to d -wave and f -wave types. Our results may provide a theoretical scenario for a recent experiment where it was observed that superconductivity in the MoTe_2 Weyl semimetal depends on the applied strain of the system⁶⁵. By diagonalizing the Bogoliubov-de Gennes Hamiltonian and deriving the corresponding wavefunctions^{28,29} (without any simplifying approximations²⁷), we also found the supercurrent flow within a Josephson junction comprised of a ballistic Weyl semimetal. We demonstrated that a Weyl semimetal Josephson junction presents a practical platform to create a device that has several tunable parameters which control the direction and periodicity of supercurrent flow, induce multiple $0-\pi$ crossovers in the critical charge current, and generates a φ_0 Josephson state.

ACKNOWLEDGMENTS

M.A. is supported by Iran's National Elites Foundation (INEF). K.H. is supported in part by ONR and a grant of HPC resources from the DOD HPCMP.

- ¹ H.Z. Weyl, *Elektron und Gravitation. I Physik* **56**, 330 (1929).
- ² N.P. Armitage, E.J. Mele, and Ashvin Vishwanath, *Weyl and Dirac semimetals in three-dimensional solids*, *Rev. Mod. Phys.* **90**, 015001 (2018)
- ³ M. Z. Hasan and C. L. Kane, *Colloquium: topological insulators*, *Rev. Mod. Phys.* **82**, 3045 (2010); X.-L. Qi and S.-C. Zhang, *Topological insulators and superconductors*, *Rev. Mod. Phys.* **83**, 1057 (2011).
- ⁴ S.-M. Huang, *etal.*, *A Weyl Fermion semimetal with surface Fermi arcs in the transition metal monpnictide TaAs class*, *Nat. Comm.* **6**, 7373 (2015).
- ⁵ B. Q. Lv, H. M. Weng, B. B. Fu, X. P. Wang, H. Miao, J. Ma, P. Richard, X. C. Huang, L. X. Zhao, G. F. Chen, Z. Fang, X. Dai, T. Qian, and H. Ding, *Experimental discovery of Weyl semimetal TaAs*, *Phys. Rev. X* **5**, 031013 (2015).
- ⁶ I. Belopolski, S. Y. Xu, D. S. Sanchez, G. Chang, C. Guo, M. Neupane, H. Zheng, C. C. Lee, S. M. Huang, G. Bian, N. Alidoust, T. R. Chang, B. K. Wang, X. Zhang, A. Bansil, H. T. Jeng, H. Lin, S. Jia, and M. Z. Hasan, *Criteria for directly detecting topological Fermi arcs in Weyl semimetals*, *Phys. Rev. Lett.* **116**, 066802 (2016).
- ⁷ A. A. Burkov and L. Balents, *Weyl semimetal in a topological insulator multilayer*, *Phys. Rev. Lett.* **107**, 127205 (2011).
- ⁸ A. A. Soluyanov, D. Gresch, Z. Wang, Q. Wu, M. Troyer, X. Dai, and B. A. Bernevig, *Type-II Weyl semimetals*, *Nature (London)* **527**, 495 (2015).
- ⁹ S.-Y. Xu, N. Alidoust, G. Chang, H. Lu, B. Singh, I. Belopolski, D. Sanchez, X. Zhang, G. Bian, H. Zheng, M.-A. Husanu, Y. Bian, S.-M. Huang, C.-H. Hsu, T.-R. Chang, H.-T. Jeng, A. Bansil, V. N. Strocov, H. Lin, S. Jia, M. Z. Hasan, *Discovery of Lorentz-violating Weyl fermion semimetal state in LaAlGe materials*, [arXiv:1603.07318](https://arxiv.org/abs/1603.07318).
- ¹⁰ F. Detassis, L. Fritz, and S. Grubinskas, *Collective effects in tilted Weyl cones: Optical conductivity, polarization, and Coulomb interactions reshaping the cone*, *Phys. Rev. B* **96**, 195157 (2017).
- ¹¹ S. P. Mukherjee and J. P. Carbotte, *Absorption of circular polarized light in tilted type-I and type-II Weyl semimetals*, *Phys. Rev. B* **96**, 085114 (2017).
- ¹² S. P. Mukherjee and J. P. Carbotte, *Imaginary part of Hall conductivity in a tilted doped Weyl semimetal with both broken time-reversal and inversion symmetry*, *Phys. Rev. B* **97**, 035144 (2018).
- ¹³ K. Halterman, M. Alidoust, and A. Zyuzin, *Epsilon-near-zero response and tunable perfect absorption in Weyl semimetals*, *Phys. Rev. B* **98**, 085109 (2018).
- ¹⁴ S. A. Yang, H. Pan, and F. Zhang, *Dirac and Weyl superconductors in three dimensions*, *Phys. Rev. Lett.* **113**, 046401 (2014).
- ¹⁵ F. Setiawan, W. S. Cole, J. D. Sau, and S. Das Sarma, *Transport in superconductor-normal metalsuperconductor tunneling structures: Spinful p-wave and spin-orbit-coupled topological wires*, *Phys. Rev. B* **95**, 174515 (2017); F. Setiawan, A. Stern, E. Berg, *Topological superconductivity in planar Josephson junctions—narrowing down to the nanowire limit*, [arXiv:1902.11300](https://arxiv.org/abs/1902.11300).
- ¹⁶ A. Fornieri, A. M. Whiticar, F. Setiawan, E. P. Marn, A. C. C. Drachmann, A. Keselman, S. Gronin, C. Thomas, T. Wang, R. Kallaher, G. C. Gardner, E. Berg, M. J. Manfra, A. Stern, C. M. Marcus, F. Nichele, *Evidence of topological superconductivity in planar Josephson junctions*, [arXiv:1809.03037](https://arxiv.org/abs/1809.03037).
- ¹⁷ A. Matos-Abiague, J. Shabani, A. D. Kent, G. L. Fatin, B. Scharf, I. uti, *Tunable magnetic textures: From Majorana bound states to braiding*, *Solid State Commun.* **262**, 1 (2017).
- ¹⁸ T. Zhou, N. Mohanta, J. E. Han, A. Matos-Abiague, I. Zutic, *From spintronics to Majorana bound states*, [arXiv:1901.02506](https://arxiv.org/abs/1901.02506).
- ¹⁹ Y. Qi, *etal.*, *Superconductivity in Weyl semimetal candidate MoTe₂*, *Nature Comm.* **7**, 11038 (2016).
- ²⁰ S.-Y. Xu, I. Belopolski, N. Alidoust, M. Neupane, G. Bian, C. Zhang, R. Sankar, G. Chang, Z. Yuan, C.-C. Lee, S.-M. Huang, H. Zheng, J. Ma, D. S. Sanchez, B. Wang, A. Bansil, F. Chou, P. P. Shibayev, H. Lin, S. Jia, and M. Z. Hasan, *Discovery of a Weyl fermion semimetal and topological Fermi arcs* *Science* **349**, 613 (2015).
- ²¹ M.D. Bachmann, N. Nair, F. Flicker, R. Ilan, T. Meng, N.J. Ghimire, E.D. Bauer, F. Ronning, J.G. Analytis, and P.J.W Moll, *Inducing Superconductivity in Weyl Semimetal Microstructures by Selective Ion Sputtering*, *Sci. Adv.* **3**, e1602983 (2017).
- ²² P. Goswami, A. H. Nevidomskyy, *Phys. Rev. B* **92**, 214504 (2015).
- ²³ G. Y. Cho, J. H. Bardarson, Y.-M. Lu, and J. E. Moore, *Superconductivity of doped Weyl semimetals: Finite-momentum pairing and electronic analog of the ³He-A phase*, *Phys. Rev. B* **86**, 214514 (2012).
- ²⁴ T. Zhou, Y. Gao, and Z. D. Wang, *Superconductivity in Weyl metals*, *Phys. Rev. B* **93**, 094517 (2016).
- ²⁵ P. Hosur, X. Dai, Z. Fang, and X.-L. Qi, *Time-reversal-invariant topological superconductivity in doped Weyl semimetals*, *Phys. Rev. B* **90**, 045130 (2014).
- ²⁶ M. Alidoust, K. Halterman, and A. A. Zyuzin, *Superconductivity in type-II Weyl semimetals*, *Phys. Rev. B* **95**, 155124 (2017).
- ²⁷ M. Alidoust, *Self-biased current, magnetic interference response, and superconducting vortices in tilted Weyl semimetals with disorder*, *Phys. Rev. B* **98**, 245418 (2018).
- ²⁸ M. Alidoust, M. Willatzen, A.-P. Jauho, *Strain-engineered Majorana zero energy modes and φ_0 Josephson state in black phosphorus*, *Phys. Rev. B* **98**, 085414 (2018).
- ²⁹ M. Alidoust, M. Willatzen, A.-P. Jauho, *Fraunhofer response and supercurrent spin switching in black phosphorus with strain and disorder*, *Phys. Rev. B* **98**, 184505 (2018).
- ³⁰ M. Alidoust, M. Willatzen, A.-P. Jauho, *Control of superconducting pairing symmetries in monolayer black phosphorus*, *Phys. Rev. B* **99**, 125417 (2019).
- ³¹ M. Alidoust, M. Willatzen, A.-P. Jauho, *Symmetry of superconducting correlations in displaced bilayers of graphene*, *Phys. Rev. B* **99**, 155413 (2019).
- ³² G. Bednik, A. A. Zyuzin, and A. A. Burkov, *Superconductivity in Weyl metals*, *Phys. Rev. B* **92**, 035153 (2015).
- ³³ R. C. Xiao, P. L. Gong, Q. S. Wu, W. J. Lu, M. J. Wei, J. Y. Li, H. Y. Lv, X. Luo, P. Tong, X. B. Zhu, and Y. P. Sun, *Manipulation of type-I and type-II Dirac points in PdTe₂ superconductor by external pressure*, *Phys. Rev. B* **96**, 075101 (2017).
- ³⁴ B. Rosenstein, B.Y. Shapiro, D. Li, I. Shapiro, *Magnetic properties of type-I and type-II Weyl semimetals in the superconducting state*, *Phys. Rev. B* **97**, 144510 (2018).
- ³⁵ Z. Hou and Q. Sun, *Double Andreev Reflections in Type-II Weyl Semimetal-Superconductor Junctions*, *Phys. Rev. B* **96**, 155305 (2017).
- ³⁶ X.-S. Li, S.-F. Zhang, X.-R. Sun, W.-J. Gong, *Double Andreev reflections and double electron transmissions in a normal-superconductor-normal junction based on type-II Weyl semimetal*, [arXiv:1805.07928](https://arxiv.org/abs/1805.07928).
- ³⁷ S.-B. Zhang, F. Dolcini, D. Breunig, B. Trauzettel, *Appearance of the universal value e^2/h of the zero-bias conductance in a Weyl semimetal-superconductor junction*, *Phys. Rev. B* **97**, 041116

- (2018).
- 38 S.-B. Zhang, J. Erdmenger, B. Trauzettel, *Chirality Josephson current due to a novel quantum anomaly in inversion-asymmetric Weyl semimetals*, [arXiv:1806.08111](https://arxiv.org/abs/1806.08111).
 - 39 A. Chen, D. I. Pikulin, and M. Franz, *Josephson current signatures of Majorana flat bands on the surface of time-reversal-invariant Weyl and Dirac semimetals*, *Phys. Rev. B* **95**, 174505 (2017).
 - 40 Y. Xu, S. Uddin, J. Wang, Z. Ma, and J.-F. Liu, *Electrically modulated SQUID with a single Josephson junction coupled by a time reversal breaking Weyl semimetal thin film*, *Phys. Rev. B* **97**, 035427 (2017).
 - 41 J. Fang, W. Duan, J. Liu, C. Zhang, and Z. Ma, *Pairing-dependent superconductivity gap and nonholonomic Andreev reflection in Weyl semimetal/Weyl superconductor heterojunctions*, *Phys. Rev. B* **97**, 165301 (2018).
 - 42 N. Bovenzi, M. Breitzkreuz, P. Baireuther, T. E. O'Brien, J. Tworzyllo, I. Adagideli, and C. W. J. Beenakker, *Chirality blockade of Andreev reflection in a magnetic Weyl semimetal*, *Phys. Rev. B* **96**, 035437 (2017).
 - 43 S. Das, Amit, A. Sirohi, L. Yadav, S. Gayen, Y. Singh, and G. Sheet, *Conventional Superconductivity in Type-II Dirac Semimetal PdTe₂*, *Phys. Rev. B* **97**, 014523 (2017).
 - 44 A. Kononov, O.O. Shvetsov, S.V. Egorov, A.V. Timonina, N.N. Kolesnikov, E.V. Deviatov, *Signature of Fermi arc surface states in Andreev reflection at the WTe₂ Weyl semimetal surface*, *EuroPhys. Lett.* **122**, 27004 (2018).
 - 45 A. Kononov, O.O. Shvetsov, S.V. Egorov, A.V. Timonina, N.N. Kolesnikov, E.V. Deviatov, *π periodicity in Josephson effect for a three-dimensional Weyl semimetal WTe₂*, *Euro. Phys. Lett.* **124**, 47003 (2018).
 - 46 S. Teknowijoyo, N. H. Jo, M. S. Scheurer, M. A. Tanatar, K. Cho, S. L. Bud'ko, P. P. Orth, P. C. Canfield, R. Prozorov, *Nodeless superconductivity in type-II Dirac semimetal PdTe₂: low-temperature London penetration depth and symmetry analysis*, *Phys. Rev. B* **98**, 024508 (2018).
 - 47 A. Sirohi, S. Das, R. R. Chowdhuri, A., Y. Singh, S. Gayen, G. Sheet, *Mixed type I and type-II superconductivity due to intrinsic electronic inhomogeneities in the type-II Dirac semimetal PdTe₂*, [arXiv:1804.10837](https://arxiv.org/abs/1804.10837).
 - 48 P. Lu, J.-S. Kim, J. Yang, H. Gao, J. Wu, D. Shao, B. Li, D. Zhou, J. Sun, D. Akinwande, D. Xing, and J.-F. Lin, *Origin of superconductivity in the Weyl semimetal WTe₂ under pressure*, *Phys. Rev. B* **94**, 224512 (2016).
 - 49 H. Takahashi, T. Akiba, K. Imura, T. Shiino, K. Deguchi, N. K. Sato, H. Sakai, M. S. Bahramy, and S. Ishiwata, *Anticorrelation between polar lattice instability and superconductivity in the Weyl semimetal candidate MoTe₂*, *Phys. Rev. B* **95**, 100501(R) (2017).
 - 50 Z. Guguchia, F. von Rohr, Z. Shermadini, A. T. Lee, S. Banerjee, A. R. Wieteska, C. A. Marianetti, B. A. Frandsen, H. Luetkens, Z. Gong, S. C. Cheung, C. Baines, A. Shengelaya, G. Taniashvili, A. N. Pasupathy, E. Morenzoni, S. J. L. Billinge, A. Amato, R. J. Cava, R. Khasanov, and Y. J. Uemura, *Signatures of the topological s^{\pm} superconducting order parameter in the type-II Weyl semimetal T_dMoTe₂*, *Nat. Comm.* **8**, 1082 (2017).
 - 51 Q. Li, C. He, Y. Wang, E. Liu, M. Wang, Y. Wang, J. Zeng, Z. Ma, T. Cao, C. Yi, N. Wang, K. Watanabe, T. Taniguchi, L. Shao, Y. Shi, X. Chen, S.-J. Liang, Q.-H. Wang, F. Miao, *Proximity-Induced Superconductivity with Subgap Anomaly in Type-II Weyl Semi-Metal WTe₂*, *Nano Lett.* (2018).
 - 52 Y. Xing, Z. Shao, J. Ge, J. Wang, Z. Zhu, J. Liu, Y. Wang, Z. Zhao, J. Yan, D. Mandrus, B. Yan, X.-J. Liu, M. Pan, J. Wang, *Surface Superconductivity in the type II Weyl Semimetal TaIrTe₄*, [arXiv:1805.10883](https://arxiv.org/abs/1805.10883).
 - 53 D. Li, B. Rosenstein, B. Ya. Shapiro, and I. Shapiro, *Effect of the type I to type II Weyl semimetal topological transition on superconductivity*, *Phys. Rev. B* **95**, 094513 (2017).
 - 54 H. Wei, S. Chao, and V. Aji, *Odd-parity superconductivity in Weyl semimetals*, *Phys. Rev. B* **89**, 014506 (2014).
 - 55 B. Lu, K. Yada, M. Sato, and Y. Tanaka, *Crossed surface flat bands of Weyl semimetal superconductors*, *Phys. Rev. Lett.* **114**, 096804 (2015).
 - 56 R. Wang, L. Hao, B. Wang, C. S. Ting, *Quantum anomalies in superconducting Weyl metals*, *Phys. Rev. B* **93**, 184511 (2016).
 - 57 Y. Li, F. D. M. Haldane, *Topological nodal Cooper pairing in doped Weyl metals*, *Phys. Rev. Lett.* **120**, 067003 (2018).
 - 58 T. Meng and L. Balents, *Weyl superconductors*, *Phys. Rev. B* **86**, 054504 (2012).
 - 59 T. Das, *Weyl semimetal and superconductor designed in an orbital-selective superlattice*, *Phys. Rev. B* **88**, 035444 (2013).
 - 60 U. Khanna, A. Kundu, S. Pradhan, and S. Rao, *Proximity-induced superconductivity in Weyl semimetals*, *Phys. Rev. B* **90**, 195430 (2014).
 - 61 E. V. Gorbar, V. A. Miransky, I. A. Shovkovy, P. O. Sukhachov, *Inter-node superconductivity in strained Weyl semimetals*, *J. Phys.: Condens. Matter* **31**, 055602 (2019).
 - 62 C. H. Wu, *Electric Field and Light Field Modulated Josephson Effect in Silicene-Based SNS Josephson Junction: Andreev Reflection and Free Energy*, *Silicon* (2019).
 - 63 T. Zhou, Y. Gao, and Z. D. Wang, *Resolving different pairing states in Weyl superconductors through the single-particle spectrum*, *Phys. Rev. B* **98**, 024515 (2018).
 - 64 A. Vasdev, A. Sirohi, M.K. Hooda, C.S. Yadav, G. Sheet, *Enhanced, homogeneous type II superconductivity in Cu-intercalated PdTe₂*, [arXiv:1903.04321](https://arxiv.org/abs/1903.04321).
 - 65 C. Heikes, I.-L. Liu, T. Metz, C. Eckberg, P. Neves, Y. Wu, L. Hung, P. Piccoli, H. Cao, J. Leao, J. Paglione, T. Yildirim, N. P. Butch, W. Ratcliff, *Mechanical control of crystal symmetry and superconductivity in Weyl semimetal MoTe₂*, *Phys. Rev. Materials* **2**, 074202 (2018).
 - 66 M. Alidoust, K. Halterman, and O. T. Valls, *Zero Energy Peak and Triplet Correlations in Nanoscale SFF Spin-Valves*, *Phys. Rev. B* **92**, 014508 (2015).
 - 67 Y. Tanaka and A. A. Golubov, *Theory of the Proximity Effect in Junctions with Unconventional Superconductors*, *Phys. Rev. Lett.* **98**, 037003 (2007).
 - 68 L. Kuerten, C. Richter, N. Mohanta, T. Kopp, A. Kampf, J. Mannhart, and H. Boschker, *In-gap states in superconducting LaAlO₃/SrTiO₃ interfaces observed by tunneling spectroscopy*, *Phys. Rev. B* **96**, 014513 (2017).
 - 69 G. Koren, T. Kirzner, Y. Kalcheim, and O. Millo, *Signature of proximity-induced $p_x + ip_y$ triplet pairing in the doped topological insulator Bi₂Se₃ by the s-wave superconductor NbN*, *EuroPhys. Lett.* **103**, 67010 (2013).
 - 70 G. Koren, *Strongly suppressed proximity effect and ferromagnetism in topological insulator/ferromagnet/superconductor thin film trilayers of Bi₂Se₃/SrRuO₃/underdoped YBa₂Cu₃O_x: a possible new platform for Majorana nano-electronics*, *Supercond. Sci. Technol.* **31**, 075004 (2018).
 - 71 M. Alidoust, A. Zyuzin, K. Halterman, *Pure Odd-Frequency Superconductivity at the Cores of Proximity Vortices*, *Phys. Rev. B* **95**, 045115 (2017).
 - 72 M. Alidoust, K. Halterman, and J. Linder, *Singlet-Triplet Superconducting Quantum Magnetometer*, *Phys. Rev. B* **88**, 075435 (2013).
 - 73 A.M. Black-Schaffer, A.V. Balatsky, *Odd-frequency superconducting pairing in multiband superconductors*, *Phys. Rev. B* **88**, 104514 (2013).

- ⁷⁴ Y. Fukaya, K. Yada, A. Hattori, Y. Tanaka, *Pairing mechanism of unconventional superconductivity in doped Kane-Mele model*, *J. Phys. Soc. Jpn.* **85**, 104704 (2016).
- ⁷⁵ Y. Fukaya, S. Tamura, K. Yada, Y. Tanaka, P. Gentile, M. Cuoco, *Inter-orbital topological superconductivity in spin-orbit coupled superconductors with inversion symmetry breaking*, *Phys. Rev. B* **97**, 174522 (2018).
- ⁷⁶ Y. Fukaya, S. Tamura, K. Yada, Y. Tanaka, P. Gentile, M. Cuoco, *Spin-Orbital Hallmarks of Unconventional Superconductors Without Inversion Symmetry*, [arXiv:1903.12379](https://arxiv.org/abs/1903.12379).
- ⁷⁷ A. Zyuzin, M. Alidoust, D. Loss, *Josephson junction through a disordered topological insulator with helical magnetization*, *Phys. Rev. B* **93**, 214502 (2016).
- ⁷⁸ I. V. Bobkova, A. M. Bobkov, A. A. Zyuzin, M. Alidoust, *Magnetolectrics in disordered topological insulator Josephson junctions*, *Phys. Rev. B* **94**, 134506 (2016).
- ⁷⁹ M. Alidoust and H. Hamzhepour, *Spontaneous supercurrent and φ_0 phase shift parallel to magnetized topological insulator interfaces*, *Phys. Rev. B* **96**, 165422 (2017).
- ⁸⁰ K. Halterman and M. Alidoust, *Half-metallic superconducting triplet spin valve*, *Phys. Rev. B* **94**, 064503 (2016).
- ⁸¹ M. Alidoust and K. Halterman, *Half-Metallic Superconducting Triplet Spin MultiValves*, *Phys. Rev. B* **97**, 064517 (2018).
- ⁸² V. Braude and Yu. V. Nazarov, *Fully Developed Triplet Proximity Effect*, *Phys. Rev. Lett.* **98**, 077003 (2007); R. Grein, M. Eschrig, G. Metalidis, and G. Schon, *Spin-Dependent Cooper Pair Phase and Pure Spin Supercurrents in Strongly Polarized Ferromagnets*, *ibid.* **102**, 227005 (2009); M. Eschrig and T. Lofwander, *Triplet supercurrents in clean and disordered half-metallic ferromagnets*, *Nat. Phys.* **4**, 138 (2008); A. Buzdin, *Direct Coupling Between Magnetism and Superconducting Current in the Josephson Junction*, *ibid.* **101**, 107005 (2008) F. Konschelle and A. Buzdin, *Magnetic Moment Manipulation by a Josephson Current*, *Phys. Rev. Lett.* **102**, 017001 (2009); Y. Tanaka, T. Yokoyama, and N. Nagao, *Manipulation of the Majorana Fermion, Andreev Reflection, and Josephson Current on Topological Insulators*, *ibid.* **103**, 107002 (2009); Y. Asano, Y. Sawa, Y. Tanaka, A. Golubov, *Odd-frequency pairs and Josephson current through a strong ferromagnet* *ibid.* **76**, 224525 (2007); A. Ozaeta, A.S. Vasenko, F.W.J. Hekking, and F.S. Bergeret, *Andreev current enhancement and subgap conductance of superconducting SFN hybrid structures in the presence of a small spin-splitting magnetic field*, *ibid.* **86**, 060509(R) (2012).
- ⁸³ A. Assouline, C. Feuillet-Palma, N. Bergeal, T. Zhang, A. Motaghizadeh, A. Zimmers, E. Lhuillier, M. Marangolo, M. Eddrief, P. Atkinson, M. Aprili, H. Aubin, *Spin-Orbit induced phase-shift in Bi₂Se₃ Josephson junctions*, *Nat. Comm.* **10**, 126 (2019).
- ⁸⁴ W. Yu, W. Pan, D. L. Medlin, M. A. Rodriguez, S. R. Lee, Zhi-qiang Bao, and F. Zhang, *π and 4π Josephson Effects Mediated by a Dirac Semimetal*, *Phys. Rev. Lett.* **120**, 177704 (2018).
- ⁸⁵ A.-Q. Wang, C.-Z. Li, C. Li, Z.-M. Liao, A. Brinkman, and D.-P. Yu, *4π -Periodic Supercurrent from Surface States in Cd₃As₂ Nanowire-Based Josephson Junctions*, *Phys. Rev. Lett.* **121**, 237701 (2018).